

Numerical modelling of hydrogen deflagrations using EXSIM

Thompson, Jamie¹[0009-0009-7732-0110] and Vembe, Bjørn Erling²[0009-0000-7560-5248]

¹ DNV Digital Solutions, Applicon House, Exchange Street, Stockport, SK3 0EY, UK

² DNV Digital solutions, Veritasveien 25, 4007 Stavanger, Norway

Abstract. The advanced gas explosion simulator EXSIM has been in active development and, subsequently, use on industrial projects since 1989. In recognition of the potentially important role that could be played by hydrogen in the energy transition, and the explosion hazards presented by accidental loss of containment of this energetic fuel, significant efforts to improve the predictive performance of EXSIM for hydrogen-air mixtures have been undertaken in recent years as part of a Joint Industry Project (JIP). In this article, the performance of the improved development version of the code is compared against that of the pre-JIP version for a series of experiments featuring a range of gas concentrations, congestion levels and degrees of confinement. The modified code is shown to display significantly improved predictive capabilities, particularly for lightly congested geometries. Further development of the model is needed in order to extend the code's capabilities to include simulation of fuel gas mixtures (e.g. hydrogen-methane fuels).

Keywords: Explosion, Hydrogen, EXSIM.

1 Introduction

Hydrogen is expected to play an increasingly important role in the global shift towards low-carbon energy systems, particularly in the transport sector [1]. As an energy carrier, hydrogen offers a number of significant benefits, including high energy content, zero emissions at the point of use, and the potential for renewable production. However, the unique characteristics of hydrogen also present significant safety challenges. It has a very wide flammability range and a low ignition energy, meaning that accidental losses of containment can be ignited with relative ease (compared with hydrocarbons), a high laminar flame speed and a propensity to undergo Deflagration to Detonation Transitions (DDTs) that can generate highly destructive overpressures [2].

In order to manage the inherent risks associated with the handling of hydrogen, it is crucial that suitable consequence models are developed to support facility design, siting and risk assessment activities. The energetic nature of hydrogen implies that gas explosion modelling must be an area of particular focus when developing/refining such modelling capabilities. Of the available modelling options in this area, Computational Fluid Dynamics (CFD) models can provide valuable additional insight due to both their

sensitivity to geometry and their ability to model flame propagation and pressure build-up in the near field.

One such model is EXSIM (EXplosion SIMulator), which is a 3D CFD code that is specifically designed for the modelling of gas explosions at industrial scales. Originally developed in the 1980s as part of a collaborative effort between Telemark Technological R&D Centre (Tel-Tek) in Norway and Shell Global Solutions in the United Kingdom, the code has been undergoing continuing development and validation as part of the KFX™ suite since 2015 [3-7]. As part of a recent Joint Industry Project (JIP), EXSIM's ability to predict pressure loads arising from hydrogen-air explosions was evaluated and improved. In this paper, the performance of the updated model is demonstrated for a series of experiments featuring a range of gas concentrations, congestion levels and degrees of confinement.

2 Model Description

2.1 Overview

At a high level, EXSIM is a finite volume CFD code based on a 3D structured cartesian mesh. The code adopts the Porosity/Distributed Resistance (PDR) method for the modelling of small scale (i.e. unresolved) obstacles in combination with a modified version of the k - ϵ turbulence model. Turbulent combustion is modelled via Magnussen and Hjertager's Eddy Dissipation Model (EDM). The code's implicit solver utilises the SIMPLE solution technique, modified to allow for compressibility effects.

In the following sections, more detailed descriptions of key aspects of the updated code are provided.

2.2 Governing Equations

To enable the efficient handling of complex geometries at industrial scales, EXSIM uses the PDR formulation originally proposed by Patankar and Spalding [8] and further developed by Sha and Launder [10]. Within the PDR framework, no effort is made to fully resolve small-scale obstacles on the computational mesh – rather, their effects on the mean flow (i.e. reduction in available flow area, application of resistance to the flow and the generation of turbulence) are modelled via the introduction of modifications to the governing flow equations.

Below, the adopted formulations for the (Favre-averaged) mass, momentum, energy and species conservation equations within the PDR framework are set out.

Mass and Momentum Conservation Equations

The continuity and momentum conservation equations are expressed within EXSIM as

$$\frac{\partial}{\partial t}(\beta_v \rho) + \frac{\partial}{\partial x_i}(\beta_i \rho U_i) = 0 \quad (1)$$

and

$$\frac{\partial}{\partial t}(\beta_v \rho U_i) + \frac{\partial}{\partial x_j}(\beta_j \rho U_j U_i) = -\beta_v \frac{\partial p}{\partial x_i} + \frac{\partial}{\partial x_j}(\beta_v \sigma_{ij}) + \beta_v \rho g_i + R_i \quad (2)$$

where:

β_v is the volume porosity

β_i is the area porosity in the x_i direction

ρ is the density (kg/m³)

U_i is the velocity component in the x_i direction

p is the pressure (Pa)

σ_{ij} is the turbulent stress tensor (kg/m·s²)

g_i is the gravitational acceleration in the x_i direction (m/s²)

R_i represents the additional flow resistance introduced by unresolved obstacles (kg/m²·s²)

As per Sha and Launder [10], the resistance per unit volume presented by a single unresolved ('subgrid') obstacle in the x_i direction is modelled as

$$R_i = -C_R A_i \left(\frac{1}{\beta_i} - 1 \right)^2 \frac{1}{2} \rho |U_i| U_i \quad (3)$$

where C_R is the drag coefficient of the solid body and A_i is its wetted area per unit volume (m²/m³).

For axial flow, C_R is set to 0.012. For crossflow, it is set to 2.0 for sharp-edged obstacles (boxes) and 1.2 for rounded obstacles (cylinders).

Energy Conservation Equation

The energy balance equation, which is derived from the first law of thermodynamics, is expressed within the PDR framework in EXSIM as

$$\frac{\partial}{\partial t}(\beta_v \rho h) + \frac{\partial}{\partial x_j}(\beta_j \rho U_j h) = -\frac{\partial}{\partial x_j}(\beta_j J_{h,j}) + \beta_v \frac{Dp}{Dt} + \beta_v S_h \quad (4)$$

where h is the enthalpy (J/kg), $J_{h,j}$ is the enthalpy diffusive flux at the boundaries of the control volume (W/m²) and S_h is the volumetric rate of heat generation due to frictional losses within the control volume (J/m³/s).

Chemical Species Conservation Equation

Finally, conservation of the mass fraction of a given chemical species, m_j , is modelled as

$$\frac{\partial}{\partial t}(\beta_v \rho m_j) + \frac{\partial}{\partial x_i}(\beta_i \rho U_i m_j) = -\frac{\partial}{\partial x_i}(\beta_i J_{j,i}) + R_j \quad (5)$$

here $J_{j,i}$ is the mass diffusive flux of species m_j and R_j is the production rate of the species within the control volume (by chemical reaction).

Turbulence Modelling

The turbulent stress tensor (σ_{ij}), and the turbulent diffusive fluxes ($J_{h,j}$ and $J_{j,i}$) introduced in Equations (2), (4) and (5) as part of the Favre-averaging process are unknowns and must be modelled in order to close the system of equations. For this, the k - ϵ turbulence model is adopted, where k represents the mean turbulent kinetic energy (m^2/s^2) and ϵ represents its rate of dissipation (m^2/s^3).

Using this approach, the turbulent stress tensor is modelled as

$$\sigma_{ij} = \mu_{eff} \left(\frac{\partial U_i}{\partial x_j} + \frac{\partial U_j}{\partial x_i} \right) - \frac{2}{3} \delta_{ij} \left(\rho k + \mu_{eff} \frac{\partial U_k}{\partial x_k} \right) \quad (6)$$

where the Kroenecker delta, δ_{ij} , is set to 1 if $i = j$ and zero otherwise.

The two diffusive fluxes are then modelled according to

$$J_{\Phi,j} = \frac{\mu_{eff}}{\sigma_\Phi} \frac{\partial \Phi}{\partial x_i} \quad (7)$$

where σ_Φ is the effective Prandtl/Schmidt number.

The effective viscosity, μ_{eff} , is then modelled as

$$\mu_{eff} = \mu_l + C_\mu \rho \frac{k^2}{\epsilon} \quad (8)$$

where the constant C_μ is taken to be 0.09.

The conservation equations for k and ϵ are then expressed as

$$\frac{\partial}{\partial t}(\beta_v \rho k) + \frac{\partial}{\partial x_j}(\beta_j \rho U_j k) = -\frac{\partial}{\partial x_j} \left(\beta_j \frac{\mu_{eff}}{\sigma_k} \frac{\partial k}{\partial x_j} \right) + G_S + G_R - \beta_v \rho \epsilon \quad (9)$$

and

$$\frac{\partial}{\partial t}(\beta_v \rho \epsilon) + \frac{\partial}{\partial x_j}(\beta_j \rho U_j \epsilon) = -\frac{\partial}{\partial x_j} \left(\beta_j \frac{\mu_{eff}}{\sigma_\epsilon} \frac{\partial \epsilon}{\partial x_j} \right) + C_1 \frac{\epsilon}{k} (G_S + G_R) - C_2 \beta_v \rho \frac{\epsilon^2}{k} \quad (10)$$

with the model constants set to:

$$C_1 = 1.44, C_2 = 1.92, \sigma_k = 1.0 \text{ and } \sigma_\epsilon = 1.3$$

The turbulence generation rates G_S and G_R in the above equations relate to contributions from shear stresses at the control volume faces and the internal frictional resistances presented by unresolved obstacles within the control volume, respectively. The component due to shear is expressed as

$$G_S = \beta_v \sigma_{ij} \frac{\partial U_j}{\partial x_i} \quad (11)$$

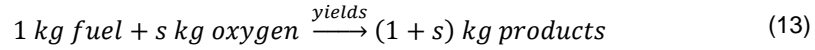
whilst the component arising from the influence of unresolved, solid obstacles is modelled following the proposal by Sha and Launder [10]:

$$G_R = C_B |U|_i |R_i| \quad (12)$$

where R_i represents the flow resistance presented by unresolved obstacles (see Equations (2) and (3)) and C_B is a modelling constant representing the fraction of the pressure drop across an unresolved obstacle that goes into the production of turbulent kinetic energy in its wake.

Combustion Modelling

Combustion is modelled in EXSIM as a single-step, irreversible reaction with a finite reaction rate between fuel and oxidiser (taken to be oxygen). Accordingly, the reaction scheme may be written as



where s is quantity of oxygen required to form a stoichiometric mixture with 1 kg of fuel. A consequence of this simple scheme is that the mixture composition can be fully determined by solving for only two variables, namely the mass fraction of fuel (m_{fu}) and the mixture fraction (f)

$$\frac{\partial}{\partial t} (\beta_v \rho m_{fu}) + \frac{\partial}{\partial x_j} (\beta_j \rho U_j m_{fu}) = \frac{\partial}{\partial x_j} \left(\beta_j \Gamma_{fu} \frac{\partial m_{fu}}{\partial x_j} \right) + R_{fu} \quad (14)$$

$$\frac{\partial}{\partial t} (\beta_v \rho f) + \frac{\partial}{\partial x_j} (\beta_j \rho U_j f) = \frac{\partial}{\partial x_j} \left(\beta_j \Gamma_f \frac{\partial f}{\partial x_j} \right) \quad (15)$$

where Γ_{fu} and Γ_f are the effective turbulent exchange coefficients (kg/m·s) and it is assumed that the Schmidt numbers are the same for all species (which is generally appropriate for turbulent flows).

The mixture fraction, f , is defined as

$$f = \frac{\xi - \xi_\infty}{\xi_0 - \xi_\infty} \quad (16)$$

where ξ is a conserved combined variable of the mass fraction of fuel, m_{fu} , and the mass fraction of oxygen, m_{o_2} , expressed as

$$f = m_{fu} - \frac{m_{o_2}}{s} \quad (17)$$

where ξ_0 and ξ_∞ are the values of ξ at fuel-rich and oxygen-rich reference points, respectively.

The mean rate of combustion referenced in (Eq. (14)) is modelled using the ‘eddy-dissipation’ concept of Magnussen and Hjertager [11], coupled with the quasi-laminar modification proposed by Van den Berg [12] as follows

$$R_{fu} = \begin{cases} \Xi \cdot \max(R_{fu,l}, R_{fu,t}), & Re_t > 2 \\ \Xi \cdot R_{fu,l}, & Re_t \leq 2 \end{cases} \quad (18)$$

where Re_t is the turbulent Reynolds number, $R_{fu,l}$ is the quasi-laminar (QL) combustion rate (kg/m³/s), $R_{fu,t}$ is the corresponding turbulent combustion rate (kg/m³/s), and Ξ is a geometry-specific flame area enhancement factor associated with unresolved obstacles.

The combustion rate associated with the quasi-laminar (QL) phase, $R_{fu,l}$, is modelled as

$$R_{fu,l} = -\beta_v C_L \rho m_{min} \quad (19)$$

where m_{min} is the smallest of the fuel, oxygen and combustion products mass fractions and the dynamic rate modelling constant, C_L , which is used to set the correct burning velocity at each timestep, is calculated using the following expression:

$$C_L = E_l \frac{\rho_u S_l m_{fu} A_f}{\int_V \rho m_{min} dV} \quad (20)$$

where ρ_u is the density of the unburnt fuel-air mixture (kg/m^3), S_l is the laminar burning velocity (m/s) and A_f is the flame area (m^2).

E_l , the flame wrinkling enhancement factor, is calculated using

$$E_l = \min(1 + k \times R, Z) \quad (21)$$

where k and Z are material-specific parameters and R is the propagation radius (m)

If the local turbulent Reynolds number is ≥ 2 , the eddy-dissipation approach, modified by Hjertager's ignition/extinction criterion [12], is used to calculate the turbulent combustion rate as follows

$$R_{fu,t} = \begin{cases} -\beta_v C_T \rho \left(\frac{\epsilon}{k}\right) m_{min}, & \frac{\tau_{ch}}{\tau_e} > D_{ie} \\ 0, & \frac{\tau_{ch}}{\tau_e} \leq D_{ie} \end{cases} \quad (22)$$

where C_T is a reaction scale factor specific to EXSIM and D_{ie} (Damköhler number) is used as the cold front quenching criterion.

Finally, the turbulent eddy mixing time-scale, τ_e , and the chemical time-scale, τ_{ch} , are defined as

$$\tau_e = \frac{k}{\epsilon} \quad (23)$$

and

$$\tau_{ch} = A_{ch} e^{\left(\frac{E}{RT}\right)} \cdot (\rho m_{fu})^a \cdot (\rho m_{O_2})^b \quad (24)$$

where A_{ch} , a and b are material-specific chemical induction time constants/exponents, E is the activation energy (J/mol), R is the universal gas constant ($\text{J/mol}\cdot\text{K}$) and T is the temperature (K).

3 Simulated Experiments

In this section, a subset of the various experiments that were used within the JIP work package for validating the model are described. The experimental campaigns targeted

within the JIP were specifically selected to include relatively ‘light’ levels of congestion for two primary reasons: firstly, such arrangements are likely to be more representative of those adopted for real hydrogen applications; and secondly, lightly congested geometries are known to be challenging for previous versions of EXSIM, as the model was originally developed for simulating scenarios in highly congested process plant.

An illustration of the utilized geometries for the various modelled experiments is presented in Fig. 1.

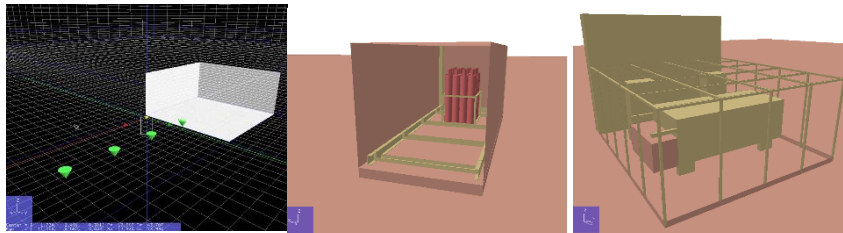


Fig. 1. View of the modelled geometric arrangements for the three example cases: Sato medium scale experiment (left pane), the HySEA homogeneous experiment (bottle rack configuration, middle pane) and the Shell hydrogen refueling station mock-up experiment (right pane).

3.1 Sato Medium Scale

This ‘open space’ test was performed as part of an experimental program that was reported by Sato et al. in 2006 [13]. The arrangement comprised nominally empty 4.3 m x 4.3 m x 2 m (37 m³) tent filled with a quiescent, stoichiometric hydrogen-air mixture.

The mixture was ignited at the center of the test rig at ground level. The experiment employed a combination of ionization pins and pressure transducers to monitor the flame front and developed pressures. The pressure transducers were located at ground level at increasing distances from the ignition point, ranging from approximately 2m (i.e. inside the fuel-air cloud) to just under 41 m.

Due to its unconfined, uncongested nature, this test provides an opportunity to assess the performance of EXSIM’s QL combustion model in isolation.

3.2 HySEA Homogeneous

The Improving Hydrogen Safety for Energy Applications (HySEA) project ran from September 2015 to November 2018 with the stated aim of providing pre-normative research on vented deflagrations in enclosures and containers for hydrogen energy applications.

Based on a review of the published data, two scenarios that were initially used in support of a blind-prediction study were selected for analysis [14]. These scenarios each involved a 20-foot ISO-container with open doors and a steel support frame installed at floor level, with one test also including a bottle basket filled with 20 50-litre cylinders.

For both tests, the container was flooded with a hydrogen-air mixture with an equivalence ratio of 0.42 and ignited at the center of the container's back wall. Three repetitions were performed for each of the two rig configurations.

3.3 Shell Hydrogen Refueling Station Mock-up

These tests were conducted in a joint effort between Shell Global Solutions (UK) and the UK Health and Safety Laboratory as part of the 'Hydrogen Safety as an Energy Carrier' (HySafe) project in 2007 [15]. The experimental setup comprised a full-scale mock-up of a hydrogen refuelling station, including a confining wall and simplified representations of a car and two dispenser units.

The test programme for the rig included a total of two distinct experiments: ignition of a hydrogen jet released from a 400 barg pressure vessel; and ignition of a near-stoichiometric hydrogen-air mixture. Pressure transducers were positioned at various locations, including on the confining wall and underneath the mock-up vehicle.

Due to EXSIM's current constraint to modelling clouds of uniform concentration, the assessment was limited to the pre-mixed cloud case (which was classified within the HySafe project as a Standard Benchmark Exercise Problem, SBEP). In this arrangement, the test rig was completely engulfed in a quiescent hydrogen-air mixture with a measured equivalence ratio of 1.09.

4 Results and discussion

This section presents and compares the predictive performance of the pre-JIP and newly updated versions of EXSIM for each of the simulated experiments. For all simulations, the grid resolution within the core combustion zone was specified in accordance with the relevant guidelines [16]. Where utilized, the maximum resolution within the region of interest outside the core combustion zone (referred to in EXSIM as the 'monitor region') was limited to 1.0 m, whilst the maximum cell size growth rate in the expansion region that serves as a buffer zone between the core and monitor regions was set to 10%.

Due to their inherent complexity, CFD models such as EXSIM do not lend themselves well to traditional approaches of appraising model uncertainty (e.g., individually assigning uncertainties to all model components and propagating these distributions through the system to yield an overall uncertainty estimate). Accordingly, the assessment was based on the model evaluation framework set out by Hanna et al. [17], which is broadly aligned with the method suggested in the Gas Explosion Model Evaluation Protocol (MEGGE) [18].

The selection of performance measures for the present work was based on the desire to indicate whether the model (in the general case) over- or underpredicts and, secondly, indicate the level of scatter in the model's predictions. Considering these requirements in tandem with the propensity for predicted and observed pressures within a given series of experiments to span several orders of magnitude, the following three commonly used fundamental measures were selected in support of the assessment:

- Geometric Mean Bias (MG)
- Geometric Variance (VG)
- Fraction of Predictions Within a Factor of Two of Observed Values (FAC2)

The geometric mean bias (MG) provides a measure of the systematic error in a model's predictions that will lead to consistent over- or underprediction, and is defined as follows:

$$MG = e^{\left(\overline{\ln\left(\frac{C_o}{C_p}\right)}\right)} \quad (25)$$

Where:

C_o is the experimentally observed value

C_p is the predicted value

The overbar indicates the mean average over all pairs of sample points (C_o and C_p)

As MG is based on the natural logarithm of the quantity of interest, it lends itself well to datasets spanning multiple decades. For a 'perfect' model, $MG = 1.0$ whilst values of $MG = 0.5$ and $MG = 2.0$ indicate a model that over- or underpredicts by a factor of two, respectively. As a guide, Chang and Hanna [19] suggest that a 'good' model would be characterised by a mean bias within $\pm 30\%$ of the mean i.e. $0.7 < MG < 1.3$. For the present work, the 95% confidence interval (CI) for MG is also calculated and reported.

The second of the adopted measures, the geometric variance (VG), indicates the degree of scatter in the model's predictions due to a combination of both systematic and random errors, and is given by:

$$VG = e^{\left(\overline{\ln\left(\frac{C_o}{C_p}\right)}\right)^2} \quad (26)$$

As per the mean bias expressed above, VG is based on the natural logarithm of the quantity of interest and therefore suited to strongly varying datasets. $VG = 1.0$ for a 'perfect' model and, according to Chang and Hanna, a 'good' model should be expected to achieve a random scatter within a factor of 2 to 3 of the mean (i.e. $VG < 3.3$).

Completing the set of the selected performance measures is the fraction of predictions whose values lie within a factor of two of the observed values (FAC2). The FAC2 measure offers the particular advantage that it is not excessively influenced by outliers in the dataset.

It naturally follows that $FAC2 = 1.0$ for a ‘perfect’ model; for a ‘good’ model, Chang and Hanna suggest that more than half of the predicted values should be within a factor of two of their observed counterparts (i.e. $FAC2 > 0.5$).

For each validation case, both tabulated and graphical summaries of model performance are provided as follows:

- Tabulated summaries of the selected fundamental performance measures (MG, VG and FAC2)
- Scatter plots of P_o against P_p
- Scatter plots of MG against VG

A representative P_o vs. P_p scatter plot is shown in Fig. 2 (left pane). Here, points lying on the solid line indicate perfect agreement between the model’s predictions and the experimentally observed values; points lying within the band bounded by the two dashed lines indicate agreement within a factor of two.

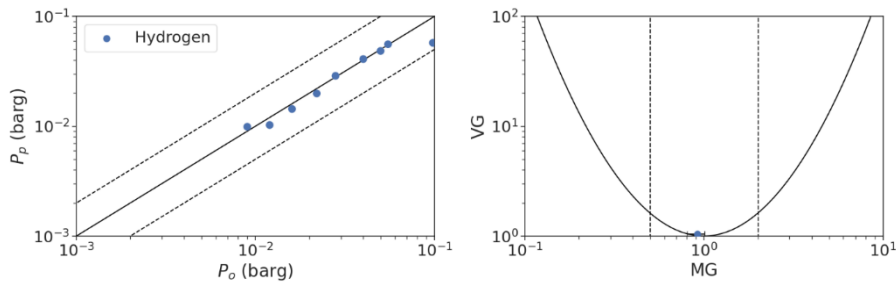


Fig. 2. Example scatter plots of P_o vs. P_p (left pane) and MG vs. VG (right pane). In this example, the results indicate a model that tends to overpredict slightly with little scatter.

A representative MG vs VG scatter plot is presented in Figure 2 (right pane). Included in the plot (and all such plots) is a solid parabola indicating the minimum theoretical variance as a function of mean bias:

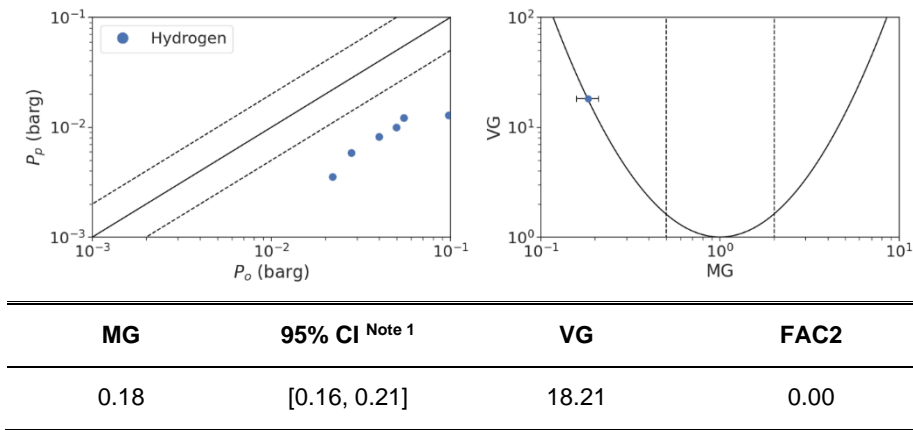
- A ‘perfect’ model would be indicated by a point at the basin of the parabola (i.e. $MG = 1.0$ and $VG = 1.0$)
- Models with points that lie on the parabola (above or below $MG = 1.0$) are observed to over- or under-predict consistently by a similar factor
- Finally, models with points that lie above the baseline defined by the parabola will over- and underpredict by a similar factor (relative to the mean bias)

Also included in plots of this type are dashed lines at $MG = 0.5$ and $MG = 2.0$ that bound the region within which the model over- or underpredicts within a factor of

two, along with lateral bars illustrating the calculated 95% confidence interval for MG.

4.1 Sato Medium Scale

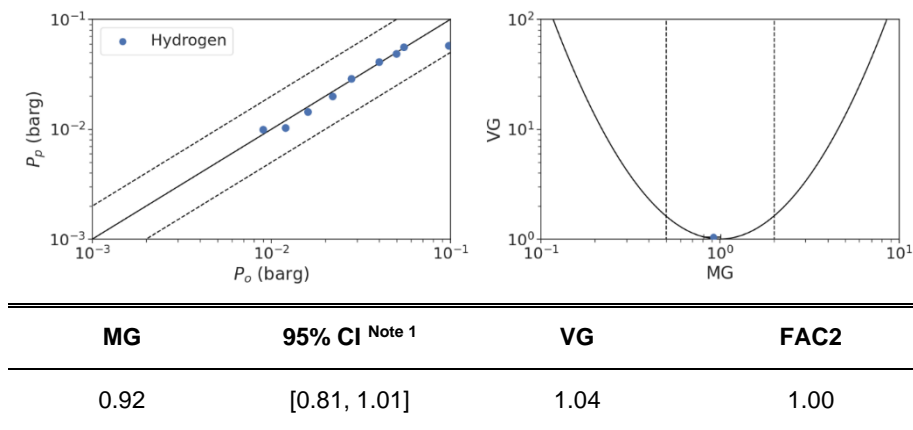
Summaries of the results obtained for direct point-by-point ‘peak pressure’ comparisons of the modelled test case are presented in Fig. 3 for the pre-JIP version of EXSIM and Fig. 4 for the updated version.



Notes:

Note 1 – 95% confidence interval (CI) for MG

Fig. 3. Validation results obtained with pre-JIP version of EXSIM for modelled Sato medium scale case (direct point-by-point comparison)



Notes:

Note 1 – 95% confidence interval (CI) for MG

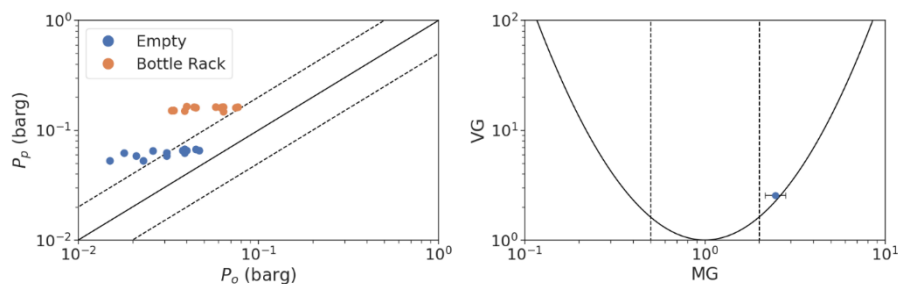
Fig. 4. Validation results obtained with updated version of EXSIM for modelled Sato medium scale case (direct point-by-point comparison)

The results for the pre-JIP version of the code for this unconfined, uncongested geometry (Fig. 3) show a significant underprediction relative to the experimentally measured values, with none of the code's predictions lying within a factor of 2 of the corresponding measurement. Due to the unconfined, uncongested nature of the experimental setup, there is insufficient turbulence generated for the code to switch over to the turbulent combustion regime, so the observed underpredictions can be directly attributed to a shortcoming in the QL combustion formulation for hydrogen.

By contrast, the predictions of the updated code (Fig. 4) are generally in excellent agreement with the experimental data. The new model can be seen to underpredict by just under a factor of two near the boundary of the fuel-air cloud and slightly overpredict at the most distant monitor location (at a range of 40.7 m). Overall, however, 100% of the updated code's predictions were assessed to be within a factor of 2 of the experimental result, demonstrating dramatically improved performance over its predecessor for hydrogen combustion modelling in the QL regime.

4.2 HySEA Homogeneous

Summaries of the results obtained using the pre-JIP and updated models for direct point-by-point 'peak pressure' comparisons of the simulated HySEA cases (which present confined, uncongested and confined, lightly congested geometries) are presented in Fig. 5 and Fig. 6, respectively.

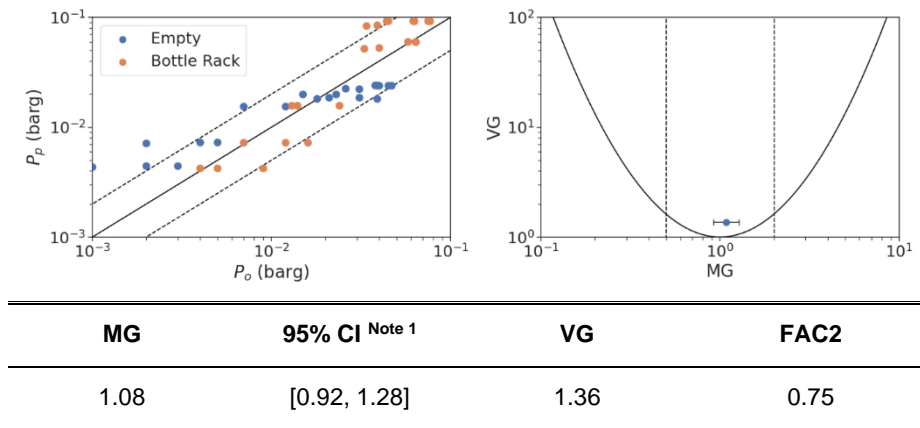


MG	95% CI ^{Note 1}	VG	FAC2
2.46	[2.16, 2.82]	2.55	0.30

Notes:

Note 1 – 95% confidence interval (CI) for MG

Fig. 5. Validation results obtained for modelled HySEA cases using pre-JIP version of EXSIM (direct point-by-point comparison)



Notes:

Note 1 – 95% confidence interval (CI) for MG

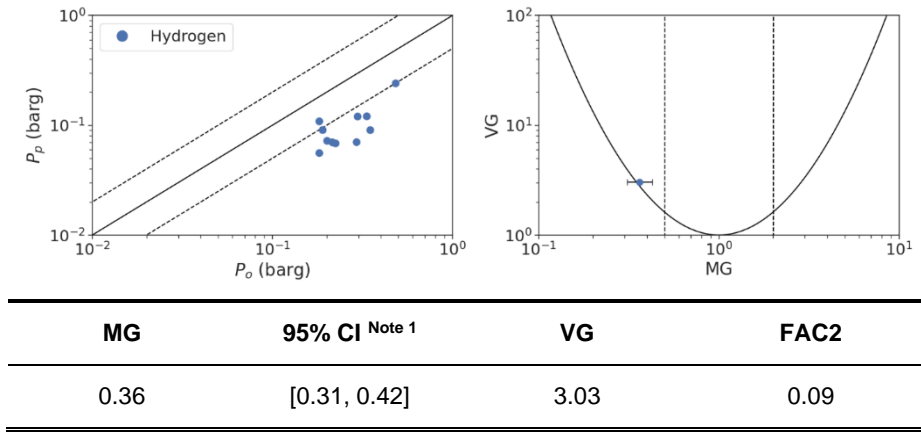
Fig. 6. Validation results obtained for modelled HySEA cases using updated EXSIM (direct point-by-point comparison)

The pre-JIP version of the code shows a clear tendency to overpredict for both test configurations, with a more severe degree of overprediction evident for the bottle rack arrangement. The correct trends are, however, predicted as the congestion level is varied, with higher pressures obtained for the cases including the bottle rack. Overall, the code's predictions were found to lie within a factor of two of the experimental result approximately 30% of the time, which is below the suggested threshold of 50% for a 'good' model.

The results for updated code indicate good performance well for both configurations, albeit with a tendency to overpredict in the far-field for the nominally empty ISO container case. It should be noted, however, that the largest deviations were found to be associated with an individual experiment ('Test 5') whose results clearly differed from two other nominally identical tests in the series. Furthermore, the code predicts the correct trends as the congestion level is varied, with higher pressures obtained for the cases including the bottle rack. Overall, the updated code's predictions were found to lie within a factor of two of the experimental result 75% of the time.

4.3 Shell Hydrogen Refueling Station Mock-up

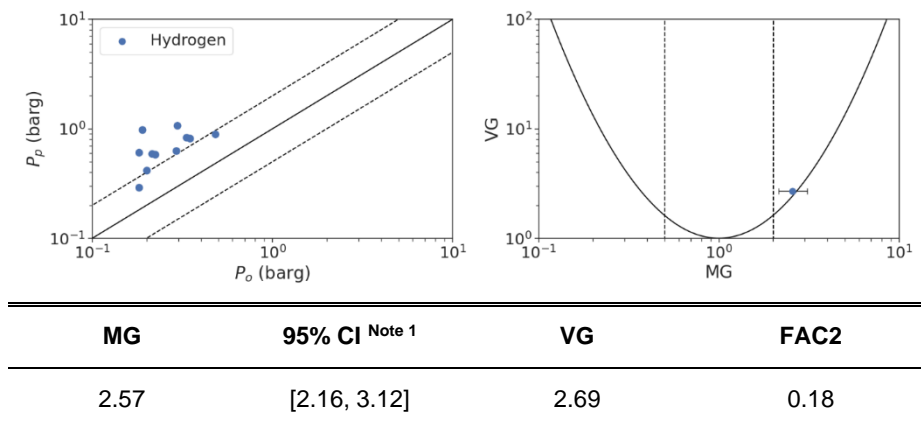
A summary of the results obtained for direct point-by-point 'peak pressure' comparisons of the modelled test case, which presents an unconfined, lightly congested geometry) using the pre-JIP version of EXSIM is presented in Fig. 7, below. The corresponding results for the updated version of the code are presented in Fig. 8.



Notes:

Note 1 – 95% confidence interval (CI) for MG

Fig. 7. Validation results obtained for modelled Shell/HSL hydrogen refueling station mock-up case for pre-JIP version of EXSIM (direct point-by-point comparison)



Notes:

Note 1 – 95% confidence interval (CI) for MG

Fig. 8. Validation results obtained for modelled Shell/HSL hydrogen refueling station mock-up case for updated EXSIM (direct point-by-point comparison)

The results indicate that the code significantly underpredicts for this test, with under-predictions exceeding a factor of two observed at almost all transducer locations (both within and outside the boundaries of the initial, quiescent fuel-air cloud).

Consequently, only 9% of the code's predictions were found to lie within a factor of two of their experimentally measured counterparts.

The results obtained for the updated code exhibit the opposite trend to this produced by the pre-JIP version. Here, it can be seen that the updated code significantly overpredicts at the majority of the considered measurement points for this case, with only 18% of predictions landing within a factor of two of the experimentally measured values and the worst of the overpredictions were observed at the most remote transducer locations. This outcome highlights a further area for model improvement, though it should be noted that the revised model, whilst still generally producing predictions that deviate from the measured values by more than a factor of two, is at least producing predictions that are conservative (which is important from a risk assessment perspective).

5 Conclusions

The performance of an updated version of KFX's gas explosion module, EXSIM, for hydrogen explosions has been assessed against a series of experimental campaigns involving lightly congested geometries.

The updated model was found to generally perform very well across the set of modelled validation cases, including measurement locations in the far-field. This represents a dramatic improvement in predictive performance relative to the initial version, which showed strong tendencies to under- or overpredict for lightly congested and confined, congested geometries, respectively, and was poorly suited for far-field computations. Unlike the initial version, the code was also found to demonstrate excellent stability for all modelled cases.

However, a significant degree of overprediction was observed in the updated model's peak pressure predictions for the Shell hydrogen refueling station mock-up test case. Work to identify and address the cause of this deviation is underway.

References

1. Gomonov K, Permana CT, Handoko CT. The growing demand for hydrogen: current trends, sectoral analysis, and future projections. *J. Unconv. Resour.* 2025; 6:100176.
2. Yang F *et al.* Review on hydrogen safety issues: Incident statistics, hydrogen diffusion, and detonation process. *Int. J. Hydrogen Energy* 2021;46:31467-31488.
3. Hjertager B. Simulation of gas explosions. *Model. Identif. Control* 1989;10:227-247.
4. Hjertager BH, Solberg T, Nymoen KO. Computer modelling of gas explosion propagation in offshore modules. *J. Loss Prev. Process Ind.* 1992;5:165-174.
5. Savill AM and Solberg T. Some improvements to PDR/k- ϵ model predictions for explosions in confined geometries. In: Perkins RJ and Belcher SE (eds), *Proceedings of the IMA/ERCOTAC Conference on Flow and Dispersion Through Groups of Obstacles*. IMA Conference Series 1994; 62: 227–249.
6. Mogenson S, Hjertager BH, Solberg T. Investigation of gas explosions in open geometries in EXSIM. In: *International Conference and Workshop on Modelling the Consequences of Accidental Releases of Hazardous Materials*. San Francisco, California, October 2000.
7. Rian *et al.* Coherent computational analysis of large-scale explosions and fires in complex geometries from combustion science to a safer oil and gas industry. *Chemical Engineering Transactions* 2016;48:175-180.
8. Patankar SV and Spalding DB. A calculation procedure for the transient and steady-state behavior of shell-and-tube heat exchangers. In: Afgan NH and Schlünder EV (eds.), *Heat Exchangers: Design and Theory* So
9. urcebook. McGraw-Hill, New York, 1974; pp 155-176.
10. Sha WT and Launder BE. A model for turbulent momentum and heat transport in large rod bundles. *Argonne Lab. Rep. AN-7-73*; 1979.
11. Magnussen BF, Hjertager BH. On mathematical modelling of turbulent combustion with special emphasis on soot formation and combustion. *Symposium (International) on Combustion*, 16;1:719-729.
12. Sæter O. Modelling and simulation of gas explosions in complex geometries [dissertation]. Trondheim, Norway: NTNU; 1998.
13. Sato Y *et al.* Experiments on hydrogen deflagration. *J. Power Sources* 2006; 159:144–148.
14. Skjold T *et al.* Blind prediction: Estimating the consequences of vented hydrogen deflagrations for homogeneous mixtures in 20-foot ISO containers. *Int. J. Hydrogen Energy* 2019; 44:8997–9008.
15. Makarov D *et al.* An inter-comparison exercise on CFD model capabilities to predict a hydrogen explosion in a simulated vehicle refuelling environment. *Int. J. Hydrogen Energy* 2009; 34:2800–2814.
16. DNV. EXSIM V7.0: EXSIM User Manual, 2025.
17. Hanna SR, Messier LL, Schulman LL. *Hazard Response Modeling Uncertainty (A quantitative method): Final Report*. Lexington MA, USA: Sigma Research Corporation; 1988.
18. Model Evaluation Group Gas Explosions (MEGGE). *Gas Explosion Model Evaluation Protocol: Technical Report, Version 1*. 1996.
19. Hanna S, Chang J. Air quality model evaluation. *Meteorol. Atmos. Phys.* 2004; 87(1-3):167–196.

Acknowledgements

The authors would like to thank Equinor for their valuable support throughout the Joint Industry Project.